Deep–Sea Research II 212 (2023) 105338

Contents lists available at ScienceDirect

Deep-Sea Research Part II

journal homepage: www.elsevier.com/locate/dsr2

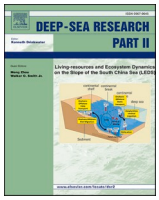

Export of Dissolved Organic Carbon (DOC) compared to the particulate and active fluxes near South Georgia, Southern Ocean

Elisa Lovecchio [a,*], Louis Clément [a], Claire Evans [a], Rachel Rayne [b], Cynthia Dumousseaud [b], Saeed Roshan [c], Sarah L.C. Giering [a], Adrian Martin [a]

[a] National Oceanography Centre, European Way, Southampton, SO14 3ZH, UK
[b] Ocean and Earth Science, University of Southampton, National Oceanography Centre, Southampton, SO14 3ZH, UK
[c] Earth Research Institute, University of California, Santa Barbara, 93117, USA

ARTICLE INFO

Handling Editor: Prof. J Aristegui

Keywords:
Biological pump
Dissolved organic carbon
Water mixing
Southern ocean
South Georgia

ABSTRACT

Quantifying the relative contributions of the export of particulate organic carbon (POC), dissolved organic carbon (DOC) and active fluxes by migrating organisms is essential to understand the functioning and vulnerability of the ocean's biological pump. However, these fluxes are rarely measured at the same time. Here we provide a first simultaneous comparison of these biological pump components in the region of South Georgia. We use a combination of in-situ data and an inverse model to calculate the DOC export and the suspended POC export and compare them to the sinking POC and active export. We find that, in this region, the DOC total export contributes about 6.6% (23.0–37.5 mg C m^{-2} day^{-1}) to the total export flux, the active flux has no discernible contribution, and the sinking POC flux is dominant with a mean value of 409 mg C m^{-2} day^{-1}. Diapycnal fluxes of DOC obtained from the cruise data constitute only a minor fraction (0.05–1.28 mg C m^{-2} day^{-1}) of the total DOC export estimated by the inverse model and are exceeded on average by the diapycnal flux of suspended POC. Our results also indicate that the total export of DOC is driven by isopycnal transport. Future fieldwork in the region of South Georgia should focus on quantifying the isopycnal flux of DOC. Future measurement campaigns should also aim to simultaneously measure the particulate, dissolved and active components of the biological pump at contrasting locations and at different times to resolve the variability of their relative contribution.

1. Introduction

The export of carbon from the surface ocean to the ocean's interior is a key component of the global carbon cycle as it exerts a fundamental control on atmospheric CO_2 concentrations (Kwon et al., 2009; Lam et al., 2011). Biological activity significantly contributes to this export via a set of processes commonly known as the "biological pump", which can be summarised by the cycle of production, export and remineralization of the organic carbon (Sarmiento and Gruber, 2006). Photosynthetic production by phytoplankton draws down dissolved inorganic carbon (DIC) concentrations in the near-surface, sun-lit layer of the ocean, storing carbon in its organic form. A portion of this organic carbon escapes the near-surface via a variety of processes such as gravitational sinking, mixing, and advection, as well as active transport by vertically migrating organisms, and is transferred deeper into the ocean before being remineralised back into its inorganic constituents, potentially resulting in the long-term sequestration and storage of carbon in the ocean.

Organic carbon accumulates in the ocean in the form of a variety of compounds, which can be roughly classified as either particulate organic carbon (POC, which is retained on a filter with a poresize of 0.2–0.7 μm) or dissolved organic carbon (DOC, which passes a filter with a poresize of 0.2–0.7 μm). The bulk of the POC concentration is in the suspended fraction (>94%; Baker et al., 2017) with the remainder comprising sinking particles. In terms of export fluxes, the vertical sinking flux of POC has been traditionally assumed to dominate the export flux of organic carbon and to be, therefore, the main driver of carbon sequestration (Ducklow et al., 2001; Suess, 1980; Turner, 2015). Sinking POC - which may comprise alive and dead cells, faecal pellets and aggregates - sinks vertically at speeds that range from 1 m per day to several hundred metres per day. This sinking flux is the most studied component of the biological pump, and is often used as a proxy to assess the global

* Corresponding author.
E-mail address: elisa.lovecchio@noc.ac.uk (E. Lovecchio).

https://doi.org/10.1016/j.dsr2.2023.105338
Received 19 August 2022; Received in revised form 28 June 2023; Accepted 25 September 2023
Available online 2 October 2023
0967-0645/

magnitude and evolution of the organic carbon export (Bisson et al., 2020; Henson et al., 2022).

Another important contribution to the export of organic material from the surface is that associated with vertically migrating organisms such as zooplankton and fish, which is termed 'active flux'. These organisms graze living and non-living POC in the near-surface, typically at night-time, and retreat to the deep ocean during the remainder of the day, in a process known as 'diurnal vertical migration' (DVM). Respiration and excretion at depth contribute to the vertical pumping of carbon to the deep ocean (Steinberg and Landry, 2017; Saba et al., 2021).

On the other hand, DOC and suspended POC require physical advection and mixing to escape the near-surface and are therefore more likely to be remineralised at shallow depths in quiescent regions, resulting in the outgassing of DIC back into the atmosphere (Berelson, 2001; Del Giorgio and Duarte, 2002). As a result, these components of the organic carbon pool have long been under-sampled or disregarded in the study of the biological pump (Buesseler et al., 2007; Hansell and Carlson, 2001, 2014). Yet, suspended POC strongly dominates POC concentrations in the near surface (Baker et al., 2017) and DOC is by far the most abundant type of organic carbon in the ocean (Hansell and Orellana, 2021; Barrón and Duarte, 2015; Hansell et al., 2009). The DOC contribution to export has been estimated to be between 10% and 30% on a global scale (Hansell, 2002, 2009; Arístegui et al., 2002; Carlson et al., 2010). The majority of DOC is generated in the near-surface layer of productive waters, especially equatorial and coastal upwelling regions, largely by primary production but also by a variety of other processes such as partial ("sloppy") feeding, viral cell lysis and the breakage of POC (Wagner et al., 2020; Hansell and Orellana, 2021). It can be laterally redistributed across the ocean by large- and small-scale currents. Vertical export of DOC happens via either large- or small-scale subduction (e.g., deep mixed layer formation and vertical transport associated with eddies and fronts respectively) and via vertical mixing, both isopycnal, i.e., by diffusion along density layers, and diapycnal, i.e., by turbulent diffusion across density layers (Hansell, 2002; Stukel and Ducklow, 2017). The latter has been previously shown to be able to export significant amounts of DOC in subtropical regions (Santana-Falcón et al., 2017). Mixing may be especially important at high latitudes, where large amounts of DOC, as well as POC, are injected at depth during periods of low stratification, remaining trapped there during the successive shoaling of the mixed layer (Dall'Olmo et al., 2016; Dall'Olmo and Mork, 2014; Giering et al., 2016; Hansell and Carlson, 2001). Subduction below the mixed layer via Ekman pumping, isopycnal eddy diffusion and lateral transport across tilted mixed layer depths is also an effective means of injection of dissolved tracers at depth at high latitudes (Sallée et al., 2010; Portela et al., 2020). While high-latitudes of the northern hemisphere receive DOC from the subtropical gyres via western boundary currents and hence have relatively high surface DOC concentrations, the Southern Ocean is characterised by relatively low surface concentrations of DOC available for export (Hansell and Carlson, 2001; Hansell, 2002; Hansell et al., 2009). Furthermore, in large parts of the Southern Ocean, wind-induced deep upwelling along the Antarctic circumpolar front potentially results in short carbon sequestration times and the inefficient export of dissolved tracers (DeVries and Weber, 2017; Siegel et al., 2021). The relative contribution of the export of DOC to the total organic carbon flux in the Southern Ocean is therefore unclear.

Quantifying the relative role of the different components of the ocean's biological pump to the total carbon export and sequestration is an essential step to understand the dynamics of the global carbon cycle and its vulnerability to perturbations. The distinct regional and seasonal variability of each pump component add complexity to this challenge. Recent efforts have tried to quantify such relative contributions, although with quite different conclusions. Using a compilation of data, Boyd et al. (2019) estimated the non-sinking components of the biological pump to contribute about 40% to the total carbon export fluxes and as much as 50% to the carbon storage, although with large uncertainties. A recent study based on model-assimilated data has provided a global estimate of the relative contribution of the sinking (70%), active (10%) and mixing (20%) components of the export flux (Nowicki et al., 2022). With a similar approach, Stukel et al. (2022) showed that most organic carbon export is driven by sinking and mixing fluxes over active fluxes, although the ratio of the contribution of the three export pathways is region-specific. Focusing specifically in the Southern Ocean and using published data of vertical gradients of organic and inorganic nitrogen, Stukel and Ducklow (2017) estimated total mixing (diapycnal + isopycnal) to contribute to 3–6% of the biological pump. This result agrees with the model-based estimate of the total DOC to total carbon export by Roshan and DeVries (2017), which is between 2 and 4% for the Antarctic and sub-Antarctic regions as a whole. However, to our knowledge, no observational program has yet estimated and compared these different organic carbon flux components simultaneously, which is essential to minimise biases in their relative contribution due to the different interannual and seasonal fluctuations of each flux.

In this work, we use data from the COMICS cruise DY086 (November–December 2017) combined with output from the inverse model of Roshan and DeVries (2017) and data from the Hansell et al. (2021) dataset to calculate the diapycnal and total export flux of DOC and the export of suspended POC in the region of South Georgia (Southern Ocean). We compare these fluxes with the sinking POC and active fluxes measured during the same field campaign (Giering et al., 2023; Cook et al., 2023 – both this issue). This approach allows us to simultaneously quantify the relative contribution of the dissolved, particulate and active components of the biological pump for the first time using in-situ data collected during the same field campaign.

2. Material and methods

The COMICS cruise DY086 collected data between mid-November and mid-December 2017 in the region of South Georgia (Fig. 1). The measurement station is located just south of the polar front and is crossed by the flow of the Southern Antarctic Circumpolar Current (SACC), in a region of high productivity and net vertical downwelling (Marshall and Speer, 2012; Matano et al., 2020; Sallée et al., 2010). To carry out a comparison of the export fluxes it is important to choose a common depth for the comparison. Giering et al. (2023) identified an export depth of 95 m which they subsequently used for sinking particle flux analysis. This export depth corresponds to the productive layer depth, defined as the deepest point at which chlorophyll was higher than 10% of the maximum chlorophyll concentration in the same profile; this depth was always deeper than both the euphotic zone (0.1% PAR) and the seasonal mixed layer depth during the cruise period (Giering et al., 2023; Henson et al., 2023 – both this issue). We use values of the DOC and suspended POC export depth as close as possible to this number for our comparison. We will discuss the impact of these small differences in the export horizon in our discussion. This section describes the manner in which the fluxes are estimated at the export depth. This manuscript also presents a comparison of POC, active and DOC fluxes. The active and sinking POC fluxes for DY086 are calculated and reported in more detail elsewhere (Giering et al., 2023; Cook et al., 2023 – both this issue). For this manuscript we simply cite those fluxes at the relevant depth (see Section 2.2) and refer the reader to the source papers for details.

2.1. DOC flux

The DOC total flux comprises components that go either along or across density surfaces, also known as isopycnals, and features contributions from a range of physical processes, such as mixing and advection. In the following paragraphs we describe how we calculated the across-isopycnal (diapycnal) flux, and how we inferred the along-isopycnal (isopycnal) flux and the total flux. More information about

the details of each calculation are provided in the following subsections.

The diapycnal flux is essentially vertical. It can be estimated directly using vertical profiles of DOC observations and turbulent mixing by making the standard assumption that the turbulent vertical mixing acts as an effectively diffusive process. More specifically, the vertical flux, F_{DOCv}, is given by:

$$F_{DOCv} = K_\rho \times \frac{dDOC}{dz} \quad (1)$$

where K_ρ is the "effective diffusivity" due to small scale turbulence, $\frac{d}{dz}$ is the vertical derivative and DOC is a concentration (mg C m^{-3}). Note that the flux is insensitive to the absolute value of the DOC concentration, rather it is the vertical gradient in DOC that has the influence. The method used to estimate K_ρ and the DOC vertical gradient are described in subsections 2.1.1 and 2.1.2.

In addition to diapycnal mixing, the total export flux of DOC includes isopycnal transport via advection and eddy mixing. While diapycnal mixing can be estimated using one-dimensional (i.e. vertical) analysis, isopycnal fluxes involve three-dimensional movement along sloping density surfaces. These isopycnal fluxes can be due to currents at a range of scales, spanning from basin scale (~1000 km) to mesoscale (~100 km) and sub-mesoscale (~1–10 km). Estimating the DOC total flux directly therefore requires knowledge of the local three-dimensional circulation and gradients of DOC along isopycnals. Such spatial mapping is very time-demanding and few observational programmes collect the necessary data to allow such a calculation (see Siegel et al. (2016) for an example). As the COMICS project did not carry out such spatial mapping, we instead used a three-dimensional inverse model to calculate the total DOC flux, as described in subsection 2.1.2.

2.1.1. Turbulent mixing

In recent decades, indirect fine-scale parameterizations (Kunze et al., 2006) have been developed to estimate turbulent mixing and to complement the limited amount of direct measurements using microstructure profilers (Waterhouse and Coauthors, 2014). These parameterizations assume that the internal wave-breaking primarily modulates the dissipation rate of turbulent kinetic energy, ϵ, (Polzin et al., 1995). The energy is believed to cascade from the internal wave field to smaller-scale waves before breaking into turbulence. Furthermore, the parameterizations hypothesise that the internal wave field follows the internal wave background field of the Garrett and Munk (GM) model (Munk, 1981) as found in the ocean interior away from the boundaries. In the stratified ocean interior, ϵ is inferred from the internal wave characteristics with vertical scales around 10–100 m. Assuming a mixing efficiency, Γ of 0.2 (Osborn, 1980), the diapycnal eddy diffusivity, K_ρ, is calculated from the dissipation rate using $K_\rho = 0.2\times \epsilon / N^2$ where N is the buoyancy frequency.

The parameterisation makes use of the link between properties of the circulation at larger scales and dissipation, as described above. The internal wave characteristics used are the shear and strain, which are estimated from profiles of horizontal velocity and density using LADCP (Lowered Acoustic Doppler Current Profiler) and CTD (Conductivity Temperature Depth) measurements. The shear, V_z, represents the vertical gradient of the horizontal velocity. The strain, ζ_z, quantifies the departure of the vertical stratification relative to a reference profile; it is calculated as $\zeta_z = (N^2 - N_{ref}^2)/N_{ref}^2$. The reference buoyancy frequency, N_{ref}, is estimated by using the adiabatic levelling of Bray and Fofonoff (1981) over a 400-m interval. In the shear-strain parameterisation, the internal wave field is hypothesised to predominantly affect the shear and strain at the measured vertical scales (10–100m). The shear and strain are decomposed in 200-m overlapping windows that are detrended before applying vertical wavenumber spectra. This method constrains the shallowest estimate of K_ρ at 100 m. The variance of the shear and the strain, denoted $\langle V_z^2 \rangle$ and $\langle \zeta_z^2 \rangle$, are estimated by integrating the vertical wavenumber spectra of each quantity. To remove the LADCP noise at small wavelengths, the integration is done over the ranges of 50–200 m and 25–200 m, for the shear and strain respectively, following Sheen et al. (2013), who also applied this approach to data taken in the Southern Ocean. The diffusivity becomes

$$K_\rho = K_\rho^0 \frac{\langle V_z^2 \rangle^2}{\langle V_z^2 \rangle_{GM}^2} h_1(R_\omega) j\left(\frac{f}{N}\right) \quad (2)$$

with the constant $K_\rho^0 = 0.05 \times 10^{-4} m^2 s^{-1}$. The last two terms of Eq. (2) capture the dependence on the shear-to-strain ratio (Kunze et al., 2006), R_ω, and the latitudinal dependence (Gregg et al., 2003), respectively. The shear-to-strain ratio, R_ω, represents the frequency content of an internal wave or, alternatively, the ratio of horizontal kinetic energy over potential energy (Kunze et al., 2006).

A Teledyne Workhorse Monitor 300 kHz ADCP was deployed on the CTD frame in a downward-looking position to sample 4 CTD/ADCP profiles at P3B and a total of 14 profiles at P3 (Fig. 1a). The horizontal velocities were calculated by using the velocity-inversion method (Visbeck, 2002) implemented by the LDEO IX Software (Thurnherr, 2021). In addition to the baroclinic velocities obtained from the lowered ADCP, the shipboard ADCP and the vessel GPS were used to constrain the near-surface and the barotropic velocities, respectively, to reduce the uncertainties of the baroclinic velocities (Thurnherr, 2021).

2.1.2. DOC data and vertical gradients

During DY086, DOC concentrations were measured on 4th December 2017 in the course of the second visit to the study site P3 (referred to as visit P3B) at −40.3°W −52.7°N (Fig. 1b). DOC samples were collected from Niskin bottles into high-density polyethylene (HDPE) carboys before filtration through 47-mm glass fibre filters (Whatman, pre-combusted overnight at 450 °C) and the filtered water acidified to pH 2 using ultrapure HCl (Merck Sigma-Aldrich). The filtered and acidified samples were stored at −20°C and −80°C before being analysed on land using a Shimadzu TOC-VCPN DOC and TDN analyser.

Only a single DOC vertical profile is available from DY086, making it difficult to assess robustly uncertainties on our flux estimate. To mitigate this limitation, we also used DOC data available online from the Hansell et al. (2021) dataset in the vicinity of the study site P3 (Fig. 1a). We selected DOC profiles that were measured north of the island of South Georgia, in the proximity of P3. The extra data amount to seven DOC profiles, of which three were collected during 20th-22nd January 2005 by the program U.S. Repeat Hydrography (https://cchdo.ucsd.edu/cruise/33RO200501), and four were collected during 24th-26th January 2014 by a GO-SHIP cruise (https://cchdo.ucsd.edu/cruise/33RO20131223). An analysis of the climatological mean data for chlorophyll and geostrophic currents from satellites (Fig. 1) indicated that five of the extra DOC profiles (across four locations) are located within a branch of the SACC flowing westward along the island South Georgia and then south of P3, in a region of lower mean surface productivity. The other two DOC profiles (both from the northernmost measurement point) are within the dynamically quieter but higher-chlorophyll area within the loop formed by the ACC as it passes South Georgia. We will address how the locations affect the DOC profiles in the Results section.

We use an export depth of 100 m for our DOC diapycnal flux calculation, as this is the shallowest depth at which the diffusive coefficient K_ρ could be calculated. Due to the near-linear tendency of the analysed DOC profiles in the top few hundred metres (see Results, Fig. 2), the DOC vertical gradient around the export depth was calculated as a linear regression across 0–255 m depth for DY086 and across 0–200 m depth for the Hansell dataset. While the latter is centred around the reference export depth, for DY086 we used a larger range of depths in order to maximise the number of available points (only three data points are available in the range of 0–200 m). Restricting the analysis to the shallowest three data points of DY086 to keep the regression within 0–200 m does not significantly change our results and does not affect the conclusions.

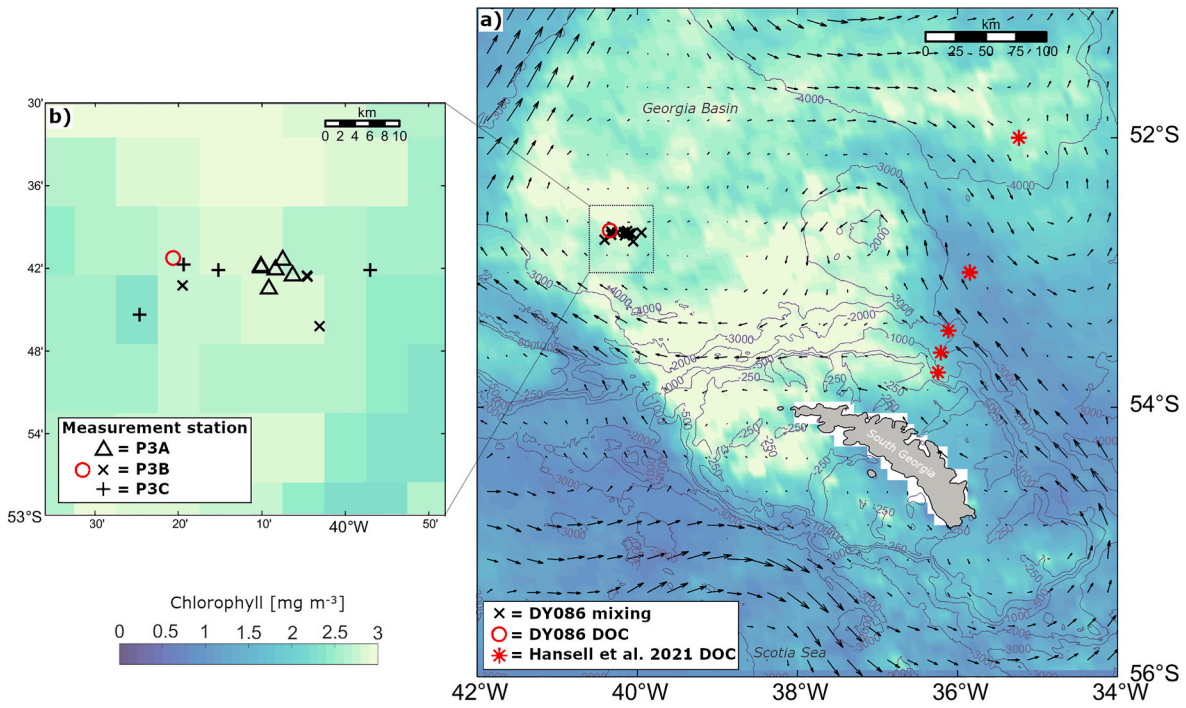

Fig. 1. Location of the data from cruise DY086 and from the Hansell et al., (2021) database on climatological mean fields for December–January. Shading: chlorophyll (SeaWiFS-IMOS L3 1998–2010, Johnson et al., 2013); vector field: geostrophic currents (DUACS L4 2005–2017 Rep ¼°, CMEMS DUACS data (2022)); contour lines: GEBCO Bathymetric Compilation Group, 2021 bathymetry [m]. (a) Location of the DY086 turbulent mixing data (black crosses), DY086 DOC data (red circle), and Hansell et al., (2021) data (red stars). Please note that the northernmost two stations from the Hansell dataset contain two DOC profiles each, at nearly the same location. The zoom-in (b) focuses on the location of the DY086 data at station P3, with symbols indicating the visit to which each profile belongs: P3A (15 - 22nd November), P3B (29th November – 5th December) and P3C (9–15th December). We used climatological mean chlorophyll fields from SeaWiFS-IMOS due to both the scarcity of clear-sky images for the measurement period (Supplementary Fig. S1) and their better representation of chlorophyll concentrations in the region of study (Johnson et al., 2013); a comparison between the geostrophic currents observed in November–December 2017 (Supplementary Fig. S1) and the climatological currents field plotted in Fig. 1a did not show any remarkable difference.

2.1.3. *DOC total flux*

We made use of an existing inverse model (Roshan and DeVries, 2017) to estimate the DOC total export flux in the area. The reader is directed to Roshan and DeVries (2017) for details but, as a quick summary, this inverse model uses an artificial neural network (ANN) to reconstruct the global distribution of DOC from the sparse data available, using relationships extracted with other parameters such as nutrients. The resulting DOC concentrations are mapped onto a 2^{o}x2° grid. By combining this map of DOC with a matrix representation of the physical circulation, itself once more constrained using hydrographic and tracer data, it is possible to estimate the creation and export of DOC in each of the inverse model grid cells. The model does not make use of the DOC data collected during DY086. Nevertheless, a comparison between the modelled DOC concentration and the DOC profiles from the in-situ data used in this manuscript shows that, in the region of focus, the modelled DOC concentration falls right in the middle of the range spun by the in-situ DOC profiles and follows an analogous vertical profile, assuring compatibility between in-situ data and model (see Supplement Fig. S2).

In order to compare the modelled DOC flux with the POC and active fluxes from COMICS DY086 data (Table 1), we used the median DOC flux from the grid cell that is closest to the DOC measurements from DY086, and estimated the modelled minimum-maximum DOC fluxes using the first and third quartiles of the simulation. Modelled DOC fluxes refer to an export depth of 114 m, which is the modelled flux depth falling closest to the POC export depth of 95 m. Note that, while our evaluation shows that modelled DOC concentrations match the in-situ DOC profiles, the model is known to fall closer to winter conditions in the physical flow at high latitudes (Roshan and DeVries, 2017), hence the estimated DOC fluxes from the inverse model are likely high-end values.

The modelled DOC total export includes both diapycnal and isopycnal DOC export. In order to explain the magnitude of the modelled total DOC flux, we compared it to the magnitude of the DOC flux components that, unlike the diapycnal mixing flux, are not resolved by the in-situ data. We estimated these fluxes from the product between the measured DOC concentration at the export depth and the estimated rate of subduction (Sallée et al., 2010), which transports water and tracers from the near-surface down into the permanent thermocline. This back-of-the-envelope calculation for the DOC subductive flux (Discussion subsection 4.2, not included in Table 2) is only aimed at explaining the difference between the total and diapycnal fluxes of DOC obtained respectively with model and data, and wants to highlight the importance of resolving the three-dimensional flow driving along-isopycnal fluxes.

2.2. *POC and active fluxes*

In the present manuscript, we calculated diapycnal mixing POC fluxes with the same approach used to calculate the diapycnal DOC flux (see subsections 2.1.1 and 2.1.2). POC exported via diapycnal mixing is mostly in the form of suspended POC, which makes up the bulk (~94%; Baker et al., 2017) of POC concentrations. We hence base our calculations on the high-resolution glider-derived total POC concentrations (calibrated against bottle samples) measured at P3B during DY086. The methods and data used to obtain the glider-derived POC concentrations are presented in full in the companion paper (Giering et al., 2023). For consistency with the diapycnal DOC flux calculation, we first calculated the regression for the POC concentration in the range of 0–200 m. However, given the highly non-linear shape of the POC curve across the 0–200 m range, we also restricted our calculation to the proximity of the

export horizon (80–120 m depth range). We used both results and multiplied them by the diffusive coefficient K_ρ to calculate the POC diapycnal export flux. Additionally, we also estimated the export of suspended POC via subduction with the same method used for DOC, as the product of POC concentration at the export depth and the rate of subduction (Sallée et al., 2010). Since this export component is only roughly estimated, we did not include it in the flux comparison table (Table 2), but we discussed its potential contribution to total export in the Discussion's subsection 4.2.

High-resolution vertical profiles of the sinking flux of POC were estimated elsewhere (Giering et al., 2023) by combining a range of independent flux measurements. Briefly, the sinking particle flux was directly measured using neutrally buoyant sediment traps (PELAGRAs) and Marine Snow Catchers deployed at 4–5 depths: typically, export depth (z_{Ex}) + 10 m, z_{Ex} + 50 m, z_{Ex} + 100 m, 250 m and 500 m. Sinking POC fluxes were also estimated from glider-derived backscatter signals (at 700 nm) and distinguished into 'large' and 'small' particles following the backscatter spike-analysis methods developed by Briggs et al. (2011). Backscatter was converted to POC concentrations using POC concentration determined from water samples collected between the surface and 1000 m depth using Niskin bottles fitted to a CTD rosette. Sinking POC fluxes were calculated by attributing distinct sinking velocities to the glider-derived 'large' and 'small' particles based on direct and indirect measurements during the cruise, and a sensitivity analysis was carried out in order to account for uncertainties in the sinking velocity estimates (for details see Giering et al., 2023 & Henson et al., 2023). The backscatter-derived sinking POC fluxes matched the direct flux observations well, allowing us to use the high-resolution glider-derived estimates for further analysis. Further details on the sinking POC flux calculations are available in the companion paper Giering et al. (2023).

The active flux was estimated by examining vertical profiles of the distribution of diurnally migrating organisms. This approach included the analysis of day and night profiles of total mesozooplankton and micronekton biomass collected via nets and acoustic backscatter data to identify any pattern indicating synchronised diurnal vertical migration; although the nets were collected only across the top 500 m of the water column, acoustic data allowed observation of scattering layers up to at least 700 m of depth. Further details and data are available in the companion paper (Cook et al., 2023).

3. Results

3.1. Diapycnal DOC flux

DOC concentrations from both DY086 and the Hansell dataset showed similar trends with depth, specifically a near-linear decrease in the first 200 m depth, followed by near constant concentrations in the lower mesopelagic zone (Fig. 2a). DOC from DY086 (Table 1) was higher at all depths compared to the Hansell profiles. This offset is likely due to a combination of factors such as the higher primary productivity and slower currents that characterise the region around P3 (DY086) compared to the locations of the Hansell dataset (Fig. 1), and, possibly, an analytical offset. This constant offset does not affect the slope of the DOC profile used for the diapycnal flux calculation. Nevertheless, we take it into account in our discussion of the DOC isopycnal flux estimate (subsection 4.2).

Linear regressions provide a gradient of 0.040 ± 0.002 mmol C m^{-4} for the DY086 DOC profile, while profiles from Hansell et al. (2021) are characterised by an average DOC gradient of 0.038 ± 0.003 mmol C m^{-4}. The average gradient over the entire set of DOC profiles is 0.039 mmol C m^{-4}, within a minimum–maximum range of 0.069–0.022 mmol C m^{-4}. Note that we use maxima and minima for uncertainties rather than standard deviations given the low number of analysed profiles.

The diapycnal diffusivity sampled during P3B at 100 m is 0.8×10^{-5} m^2 s^{-1} with a 95% confidence interval of 0.2–1.8 $\times$ 10^{-5} m^2 s^{-1}. The diapycnal diffusivity remains similar at 150 m with 1.2×10^{-5} m^2 s^{-1} before decreasing below 200 m. For all P3 profiles, the mean K_ρ shows a similar equivalent value within 100–200 m with $K_\rho = 1.1^{*} \cdot 10^{-5}$ m^2 s^{-1}, which remains constant down to 600 m and is indistinguishable from the shallow values at P3B within 100–150 m. Overall, similar K_ρ values within 100–200 m and down to 600 m indicate that K_ρ is correctly capturing the interior internal wave dynamics, away from the mixed layer dynamics, as hypothesised by the parameterisation.

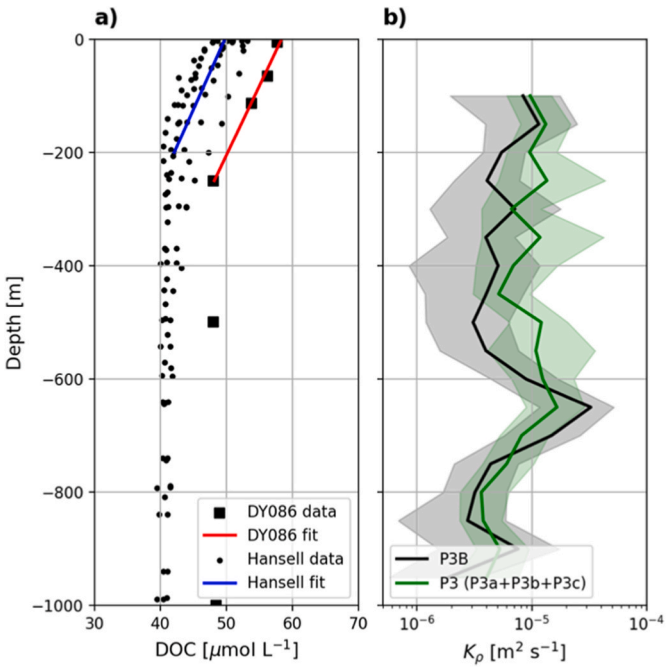

Fig. 2. (a) DOC concentrations as a function of depth from DY086 during P3B (black squares) and from the Hansell et al., (2021) dataset (black circles) with regression lines respectively in red and blue; (b) diapycnal diffusivity, K_ρ, as a function of depth averaged across the DY086 measurements during P3B only (black) and during the entire cruise (P3A, P3B, P3C) (green) with the 95% confidence intervals obtained from bootstrapping.

Table 1
DOC concentrations from the COMICS cruise DY086 collected at 40.3°W, 52.7°S on 4th/December/2017 during P3B. DOC concentrations have an uncertainty of 1.6 μmol L^{-1}.

Depth [m]	DOC [μmol L^{-1}]
8	57.8
63	56.2
114	53.8
255	48.1
504	48.1
1007	48.5

Using the mean DOC gradient and mean diffusivity parameter at 100 m gives us a mean downward diapycnal flux of DOC of 0.32 mg C m^{-2} day^{-1} (0.33 mg C m^{-2} day^{-1} when considering only the data collected during DY086). Considering the end-range values of both DOC gradient and diffusivity, we obtain minimum–maximum values of the DOC diapycnal export of 0.05–1.28 mg C m^{-2} day^{-1}.

3.2. Total DOC flux

The DOC total flux obtained from the inverse model, including both diapycnal and isopycnal fluxes, in the proximity of the measurement location P3 amounts to 29.0 mg C m^{-2} day^{-1} (10.6 g C m^{-2} yr^{-1}), with a minimum–maximum range of 23.0–37.5 mg C m^{-2} day^{-1} (8.4–13.7 g C

m^{-2} yr^{-1}) (Fig. 3). Spatial variability of the modelled DOC flux around the measurement location is relatively small, with median export fluxes in the range of 17.8–37.0 mg C m^{-2} day^{-1} (6.5–13.5 g C m^{-2} yr^{-1}). Higher values of modelled DOC export coincide with regions of high chlorophyll concentrations, i.e., north-west of South Georgia (compare Figs. 3 and 4).

3.3. Diapycnal POC flux via mixing

Glider-derived POC concentrations at P3B during DY086 (Giering et al., 2023) showed a steep decline around the export horizon (Fig. 5). A linear regression for the data collected between 0 and 200 m provides a gradient of 0.082 ± 0.009 mmol C m^{-4}. This value results in a mean export of 0.68 mg C m^{-2} day^{-1}, with minimum-maximum range of 0.15–1.70 mg C m^{-2} day^{-1}, considering the end-range values of both POC gradient and diffusivity. Restricting the regression to the range of 80–120 m, around the export depth, provides a compatible result, with a gradient of 0.097 ± 0.015 mmol C m^{-4}. This value corresponds to a mean diapycnal mixing POC export of 0.80 mg C m^{-2} day^{-1}, with a minimum-maximum range of 0.17–2.09 mg C m^{-2} day^{-1}. Given the highly non-linear shape of the POC concentration in the range of 0–200 m, we use the diapycnal mixing POC flux results obtained with the restricted range of data points, as they best represent the POC concentration gradient around the export depth.

4. Discussion

4.1. Relative role of DOC, POC and active export fluxes

Here we compare our estimates of the DOC fluxes and POC diapycnal flux with the sinking POC (Giering et al., 2023) and the active flux (Cook et al., 2023) estimates, with the aim of quantifying the relative contribution of each flux to the total export (POC + DOC + active) of organic carbon (Table 2). Our results indicate that diapycnal mixing flux of DOC represents on average less than 0.1% of the total organic carbon export, with an estimated maximum of 0.3%. This low contribution indicates that, in austral summer, diapycnal DOC export is likely not a significant component of the biological pump at this location. Total modelled DOC export, however, represents about 6.6% of the total export flux. This contribution is at the high-end of previous estimates of the average DOC export contribution across the Southern Ocean (3–6%, Stukel and Ducklow, 2017) and indicates a small, but not irrelevant, contribution of DOC to the biological pump in the region of South Georgia. Our results

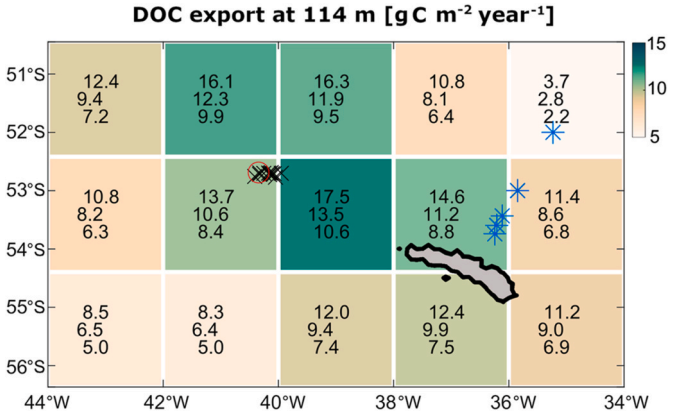

Fig. 3. Modelled DOC total export fluxes in units of g C m^{-2} yr^{-1} using output from inverse model presented in Roshan and DeVries (2017) in the study region. Measurement locations are marked as black crosses (DY086, mixing), a red circle (DY086, DOC), and blue asterisks (Hansell et al., 2021, DOC). In each square, numbers indicate: maximum export as third quartile (upper row), median export (middle row), minimum export as first quartile (lower row).

also suggest that DOC export is likely dominated by along-isopycnal transport rather than by diapycnal mixing (see subsection 4.2 for an estimate of the isopycnal export component based on the in-situ DOC data). Diapycnal mixing of POC exceeds on average the DOC diapycnal export thanks to the sharp POC concentration gradient found at the edge of the productive layer; yet overall diapycnal POC export is also very small, contributing only 0.2% to the total flux. Nonetheless, our results highlight that POC significantly contributes to turbulent export fluxes of organic carbon and must be considered in the calculation of diapycnal export fluxes.

Based on the absence of evidence for synchronised DVM, the contribution of active transport to the export of organic carbon is likely negligible (Cook et al., 2023). Asynchronous DVM may have taken place but was not resolvable by the data and is expected to be minor (Cook et al., 2023). The results of this comparative study indicate that in austral summer the biological pump in the region of South Georgia is strongly dominated by the vertical export of sinking POC, with the total export of DOC contributing only a few percent (<7%).

It is important to notice that the sinking POC flux is characterized by a rapid attenuation, particularly just below the export depth (Giering et al., 2023). Sinking POC flux at 115 m depth, which is ~20 m below the export depth but close to the modelled DOC export depth of 114 m, reaches a mean value of 285 mg C m^{-2} day^{-1} (uncertainty envelope: 81–652 mg C m^{-2} day^{-1}). If we refer our calculations to this deeper flux horizon, total carbon flux sums up to 314 mg C m^{-2} day^{-1}, with a DOC contribution of 9.2% to the total flux. This sensitivity test demonstrates that, although changing the export horizon may slightly change the percent contribution of DOC to the total organic carbon flux, the sinking POC flux remains dominant. As a result, slight variations in the choice of export horizon do not affect our conclusions.

Our results for the DOC diapycnal export, POC export and active export from in-situ data are representative of austral summer carbon fluxes in the study region, while DOC total export from the data-driven inverse model is an annual mean flux and most likely represents a high-end value due to the combination of summer-like high DOC concentrations and winter-like physical flow represented by the model (see Methods subsection 2.1.2). Our DOC total export being a high-end estimate strengthens our claim that, in austral summer, sinking POC export drives the biological pump at this location. Summing the total DOC, diapycnal POC and sinking POC export fluxes provides a total organic carbon export flux of 439 mg C m-2 day-1 (Table 2); this represents ~30% of the primary production measured at P3B during the same field campaign (Giering et al., 2023; Henson et al., 2023). Seasonal variability in the fluxes is expected to affect the contribution of the biological pump components differently: while both POC and DOC concentrations in the productive layer may fall during periods of low-productivity, physical processes driving diapycnal export are likely to strengthen in winter. DVM patterns are also known to change seasonally (Bandara et al., 2018) hence require to be resolved in time. The contribution of DOC export to total organic carbon export hence likely varies considerably throughout the seasonal cycle.

4.2. DOC flux components

As the diapycnal DOC export calculated from our in-situ data constitutes a small fraction of the DOC total flux estimated from the inverse model, it is likely that the latter involves contributions from other physical pathways. According to Sallée et al. (2010), the region around South Georgia is characterised by annual mean net subduction, meaning that at this location, on average, water leaves the near-surface and is transferred down into the interior permanent thermocline, found at the base of the winter mixed layer. At this location, subduction is mostly driven by monthly mean geostrophic transport across tilted mixed layer depths (i.e. lateral induction) and eddy diffusion, and has an annual mean rate of about 30 m $year^{-1}$ (~0.08 m day^{-1} = $1{\cdot}10^{-6}$ m s^{-1}) (Sallée et al., 2010). Argo data indicate that maximum winter mixed layer depth

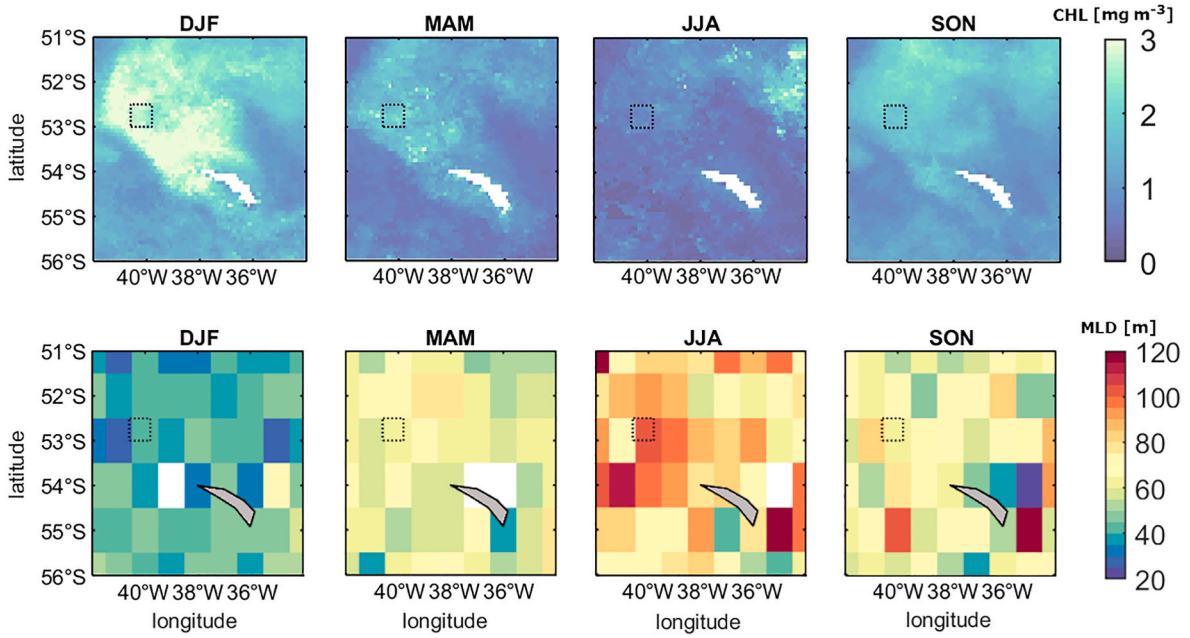

Fig. 4. Seasonal climatology of chlorophyll from satellite data (SeaWiFS-IMOS, 1998–2010, Johnson et al., 2013) and of the mixed layer depth (MLD) 1° × 1° Argo floats data (Holte et al., 2017). White areas indicate missing data, including no-data due to the presence of land.

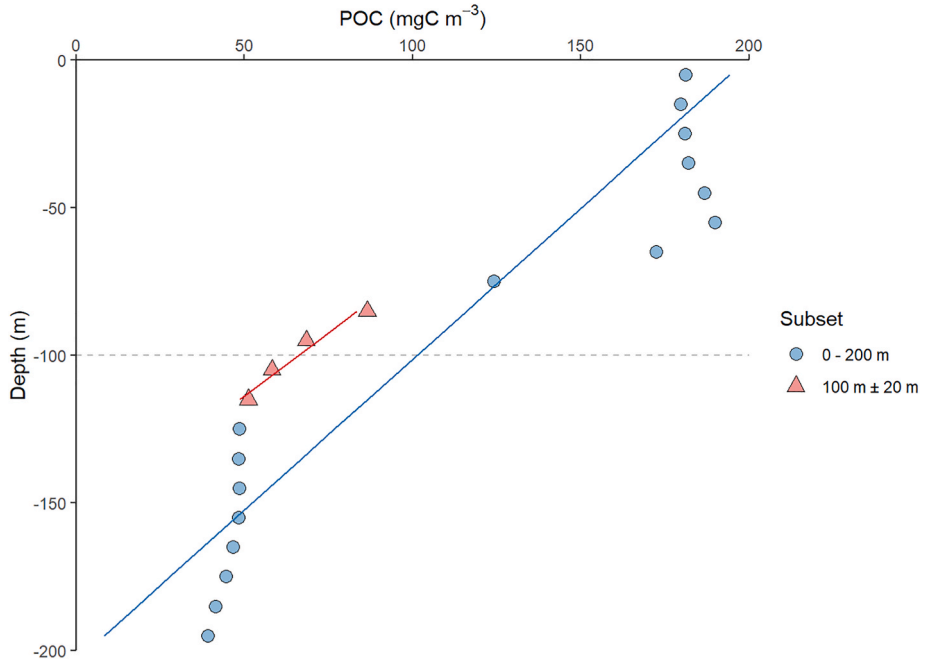

Fig. 5. Vertical profile of glider-derived POC concentrations over the top 200 m at P3B during DY086 (Giering et al., 2023). Lines show regressions for the depth range 0–200 m and 80–120 m (blue and red symbols and lines, respectively).

corresponds to about 100 m in this region (Fig. 4). A linear interpolation at 100 m depth provides a DOC concentration of 54.5 μmol L^{-1} for our dataset and of 47.7 μmol L^{-1} using the Hansell et al., (2021) dataset (Table 1, Fig. 1). The product of the mean subduction rate and the two DOC concentrations provides an estimated range of DOC export via subduction of 45.8–52.3 mg C m^{-2} day^{-1}. This rough estimate does not account for any seasonal variability or small-scale patchiness in fluxes across the permanent thermocline and likely provides an upper limit to the subductive flux due to our simplified calculation not explicitly accounting for the two-way eddy mixing component. As a consequence, the estimated range falls above the higher end of the total flux obtained via the inverse model for the grid point closest to the DOC measurement at P3B (37.5 mg C m^{-2} day^{-1}, 3rd quartile), although it matches its order of magnitude. Note that the maximum inverse model DOC total export in the grid point located just east of P3B is 47.9 mg C m^{-2} day^{-1} (17.5 g C m^{-2} yr^{-1}), which is compatible with our range of estimated subductive DOC flux. Lateral induction and along-isopycnal eddy diffusion of DOC, which drive subduction in this region (Sallée et al., 2010), are therefore likely to play a key role in driving the total export of DOC. The agreement between the magnitude of our subduction estimate and the modelled DOC total flux, and the fact that they are both likely high-end estimates, strengthens our finding that DOC export in the study

Table 2
Comparison of the organic carbon export fluxes [mg C m^{-2} day^{-1}] in austral summer at site P3 via export of DOC, POC and active transport. % Total shows the percent contribution of each mean flux to the estimated total mean flux of carbon, where the total mean flux is calculated as the sum of the mean values of DOC total export, the POC diapycnal mixing export, the sinking POC export and the active export (439 mg C m^{-2} day^{-1}).

	Carbon export [mg C m^{-2} day^{-1}]				
	DOC diapycnal export	DOC total export	POC diapycnal export	Sinking POC export	Active export
Minimum	0.05	23.0	0.17	124	–
Mean	0.32	29.0	0.80	409	Negligible
Maximum	1.28	37.5	2.09	891	–
% Total	<0.1%	6.6%	0.2%	93.2%	0%

region is significantly smaller than the POC sinking export flux.

A similarly rough estimate can be calculated for the subduction of suspended POC: using the POC concentration at 95 m depth (68.4 mg C m^{-3}, Giering et al., 2023) we obtain a subductive POC flux of 5.5 mg C m^{-2} day^{-1}, which is an order of magnitude smaller than the flux obtained for DOC and nearly 100 times smaller than the sinking POC flux, which still dominates the total organic carbon export. Due to its small magnitude, adding the subductive POC flux component to the total carbon export (Table 2) would not affect our conclusions.

Another potential contribution to the export of DOC may be that of small-scale vertical fluxes associated with ageostrophic flows at the edge of small-scale fronts or the periphery of eddies. These are at too small scales to be captured by the inverse model. These small-scale vertical fluxes have been observed to efficiently inject carbon at depth (Omand et al., 2015), although their integrated contribution may be small (Resplandy et al., 2019). An analysis of the pattern of currents in the sampled region from satellite data (Fig. 1) shows slow flow conditions across the entire high-chlorophyll region of the South Georgia basin, which is surrounded at its periphery by the faster flow of the SACC (Matano et al., 2020). Ship measurements at P3 detected currents below 0.05 m s-1 with no dominant direction (Carvalho, pers. comm.). This slow circulation (Fig. 1) is reflected in an analogous pattern of eddy kinetic energy showing low values in the productive region north-west of the island and higher values at the location of the SACC, as verified by calculating eddy kinetic energy from high resolution reanalysis data of currents in the region (CMEMS GLORYS12V1 data, 2022). Therefore, only at the outer perimeter of the high-chlorophyll region, high production and intense currents overlap (Fig. 1), potentially meaning that, along this boundary, fluxes associated with fronts and mesoscale features may play a role in vertical export. Nevertheless, at our study site and in great part of the South Georgia basin, there is lack of quantitative evidence for the importance of small-scale vertical fluxes associated with eddies and fronts in the export of DOC.

4.3. Variability of diapycnal mixing fluxes

The values of diapycnal mixing coefficient K_ρ found in this study of $\sim 10^{-5}$ m^2 s^{-1} correspond well to the typical values of the background diapycnal diffusivity of the ocean interior previously measured during austral summer at these latitudes. An observational study adopting a fine-scale parameterisation analogous to ours, found K_ρ just slightly above 10^{-5} m^2 s^{-1} in the upper 300–400 m of the Georgia Basin, mostly due to its deep and smooth bathymetry and high stratification (Naveira Garabato et al., 2004). A tracer release experiment and microstructure measurements also confirmed large-scale annual mean $K_\rho = (1.3 \pm 0.2) \cdot 10^{-5}$ m^2 s^{-1} and a summer $K_\rho = (0.75 \pm 0.07) \cdot 10^{-5}$ m^2 s^{-1}, respectively, at equivalent latitudes upstream of the Drake Passage and away from rough topography (Ledwell et al., 2011). The values only differ from our estimate by ~20%. Combining our values of diapycnal mixing and the measured DOC gradient results in a very small contribution of this component to the DOC total export flux (~1%) and to the total organic carbon export (<0.1%) in our study. For POC, this higher mixing may result in a diapycnal export that reaches at most 0.3% of the total flux. To obtain a notable contribution of the diapycnal export of DOC and POC by mixing to the total export of organic carbon in this region requires either an increase of the vertical gradient of organic carbon or an increase of the eddy diffusivity by a factor of at least 20 at the export depth.

Such a large change in the vertical gradient of DOC is unlikely to occur considering the relative stability of DOC in the ocean (Mentges et al., 2019). Our ship-based observations of DOC concentrations in the surface ocean were higher than the records by Hansell et al. (2021). These higher observations are not surprising considering that the satellite-derived climatology of Chlorophyll suggests that the P3 region is overall more productive (Figs. 1 and 4) and that the cruise occurred at the peak of the bloom (Giering et al., 2023). If we hence assume that our observed surface concentrations (56 μmol kg^{-1} at 8 m; Table 1) are at the higher end of DOC concentrations at this site and that the lower values observed by Hansell et al. (2021) are the minimum 'background' DOC concentrations at this site (40 μmol kg^{-1} at 200 m; Fig. 2a), the maximum gradient in DOC would be 0.083 mmol C m^{-4}. This value is higher than our observed gradient by a factor of 2, but still insufficient to result in a notable increase in diapycnal flux.

A significant increase in the vertical gradient of POC is also unlikely. The field campaign DY086, in fact, took place in a region that is a hotspot for biological productivity, during the productive season (Henson et al., 2023; Giering et al., 2023; see also Fig. 1). As a result, we can assume that our measured POC profile at P3B is characterised by a high-end value of the vertical gradient of concentration at the export depth.

Significantly higher values of K_ρ that could potentially increase the diapycnal export of DOC and suspended POC from the near-surface have been documented for the Southern Ocean (Naveira Garabato et al., 2004; Wu et al., 2011; Stukel and Ducklow, 2017; Meyer et al., 2015). These observations have been associated with a variety of situations and processes such as proximity to rough topography, winter deep-mixing, shear and ageostrophic currents at fronts, sea-ice interactions and strong wind conditions. Naveira Garabato et al. (2004) found that K_ρ could attain rates as high as 10^{-3}-10^{-2} m^2 s^{-1} in the proximity of rough topography due to the influence of internal waves, which are generated by tidal and geostrophic flows flowing over topographic features. This was especially the case in the region of the South Scotia Ridge, south of South Georgia, at depths below 500 m, where topographic features can shoal to the upper 1000 m. However, in regions of smoothed and deep topography such as the Georgia Basin, the upper water column should not be as strongly influenced by bottom-generated internal waves.

Another source of diapycnal turbulent mixing can be wind-forced near-inertial waves that can radiate their energy downward below the mixed layer depth (Alford and Gregg, 2001). CTD (Thompson et al., 2007) and float (Meyer et al., 2015) measurements point to the presence of enhanced K_ρ in the upper 800 m potentially arising from downward-propagating near-inertial waves subsequent to storms. This was confirmed by the seasonal modulation of K_ρ inferred from Argo float measurements (Wu et al., 2011). As our sampling at P3 largely occurred during non-storm conditions, there was no evidence for storm activity enhancing K_ρ at P3. Fortunately, an insight into the potential effect of storms was possible from an additional CTD profile taken south of South Georgia, at −40.9°E, −56.6°N, during rough weather and high-wind conditions. This CTD profile is characterised by K_ρ $\sim 10^{-4}$ m^2 s^{-1} between 100 and 150 m depth, showing therefore values that are one order of magnitude higher than those found at P3, and significantly higher than those previously observed in the same region at depths shallower than 300 m (Naveira Garabato et al., 2004). This high diapycnal mixing in the near-surface is also associated with lower K_ρ $\sim 10^{-5}$ m^2 s^{-1} in the

range of 200–500 m depth in the same CTD, indicating that such increase is likely associated with surface processes such as increased wind stress. Using this maximal K_ρ could result in a ten-fold increase in the DOC diapycnal export, amounting to roughly 12.8 mg C m^{-2} day^{-1}. Hence, diapycnal turbulent mixing during storm events may have the potential to export the equivalent of ~3% of the total export. However, such events would likely be infrequent and not prolonged in time. We conclude that, at our study site and in austral summer, diapycnal export of organic carbon by mixing is likely negligible.

4.4. Autonomy and the biological pump

Further insight into the spatiotemporal variability of the export flux components, including their seasonal variability and the integrated contribution of transient events to diapycnal export, cannot be easily achieved using only ship-based measurements, which are limited in their spatial and temporal sampling capabilities. New combined physical and biogeochemical data obtained with autonomous platform such as BGC-Argo floats (https://biogeochemical-argo.org/) as well as underwater gliders and Autosub Long Range (ALR) vehicles will help to study the integrated impact of sporadic mixing events on the Southern Ocean biological pump. Such data will allow us to better resolve sporadic changes in eddy diffusion, mixing and biogeochemical tracer concentrations, including POC. The use of state-of-the-art sensor integrations such as in situ camera systems and multi-channel ecosounders fitted on autonomous platforms together with more standard and mature bio-optical sensors can also better inform and resolve the distribution and movement of zooplankton and their respective contribution to carbon export.

Unfortunately, DOC is not among the variables measured by the BGC-Argo program. DOC sensors, although available for freshwater monitoring (e.g., the Proteus DOC sensor, Proteus Proteus user manual, 2023), are still not commonly used for ocean measurements. Most DOC data are therefore currently collected via traditional ship-board measurements, which require a high observational effort and limit the possibility to collect high-resolution, long-term data sequences. This observational gap also results in an important seasonal bias in DOC observations, especially in the Southern Ocean where most ship-board observations are collected during Austral spring and summer. As a result, DOC remains one of the least studied and understood components of the biological pump. Future programs should consider including DOC sensors on autonomous platforms, and should aim at better resolving the spatio-temporal variability of the DOC field and its associated fluxes.

5. Conclusions

For our study site near South Georgia in the Southern Ocean in austral summer, total vertical export of DOC was significantly smaller than POC export via sinking, contributing only a few percent (6.6%) to the total export flux. DOC total export, however, exceeded the contribution of the active flux by vertically migrating organisms. We showed that diapycnal DOC export contributed only a small fraction (1%) to the DOC total flux, suggesting that most of the DOC export at this site might occur via along-isopycnal transport. The diapycnal mixing export of POC was also small, accounting for only 0.2% of the total export flux, but exceeded the diapycnal export of DOC. Our study highlights the need to capture the three-dimensional nature of DOC export given the likely importance of along-isopycnal transport. Further, it highlights the importance of accounting for the export of suspended POC when calculating diapycnal mixing fluxes of organic carbon. Overall, our estimated contributions of active and mixing fluxes for the study region are substantially smaller than suggested by global estimates (30–50%; Boyd et al., 2019; Nowicki et al., 2022), highlighting the importance of resolving their spatiotemporal variability. Our study hence underlines the importance of simultaneously measuring the particulate, dissolved and active export of organic carbon at different locations and throughout the seasonal cycle. These simultaneous measurements would help to resolve the regional variability of the contribution of each component of the biological pump and to better understand the biological drivers of the export of organic carbon to the deep ocean.

Research data

DOC data from DY086 have been provided in Table 1. DOC data from the Hansell et al., (2021) dataset can be downloaded for the same region [-35.1°E,-36.3°E]x[-51.9°N,-53.8°N] at: https://explore.webodv.awi.de/ocean/biogeochemistry/dom/hansell-etal-2021/

All the DY086 (COMICS) data have been submitted to Pangaea Data Publisher with open-access license CC-BY-4.0 as "Biological carbon pump variables in the Scotia Sea, South Atlantic during an austral Spring bloom (November–December 2017)".

CRediT author statement

Elisa Lovecchio: Conceptualization, Methodology, Software, Validation, Formal analysis, Writing - Original Draft, Writing - Review & Editing, Visualization.

Louis Clément: Conceptualization, Methodology, Software, Validation, Formal analysis, Writing - Original Draft, Writing - Review & Editing, Visualization.

Claire Evans: Investigation, Data Curation, Writing - Original Draft, Supervision.

Rachel Rayne: Investigation, Data Curation, Writing - Original Draft, Writing - Review & Editing.

Cynthia Dumousseaud: Validation, Investigation, Data Curation, Writing - Original Draft, Writing - Review & Editing.

Saeed Roshan: Methodology, Software, Writing - Original Draft, Visualization.

Sarah L.C. Giering: Conceptualization, Methodology, Formal analysis, Investigation, Writing - Original Draft, Writing - Review & Editing, Visualization, Supervision, Project administration.

Adrian Martin: Conceptualization, Methodology, Resources, Writing - Original Draft, Writing - Review & Editing, Supervision, Project administration, Funding acquisition.

Declaration of competing interest

The authors declare that they have no known competing financial interests or personal relationships that could have appeared to influence the work reported in this paper.

Data availability

All the DY086 (COMICS) data are open-access on Pangaea Data Publisher, as "Biological carbon pump variables in the Scotia Sea, South Atlantic during an austral Spring bloom (November–December, 2017)"

Acknowledgements

The authors would like to thank Dr Kathryn Cook and Dr Filipa Carvalho for their valuable contributions to this manuscript. We would also like to thank Prof Stephanie Henson, Dr Edward Mawji, Dr Ilaria Stendardo and Dr Cara Nissen for their input and suggestions. Cruise DY086 was funded by and carried out through the COMICS Large Grant from the UK Natural Environment Research Council (NE/M020835/2). The authors extend their gratitude to the Captain of RRS Discovery and their team for their assistance. The DOC flux estimates and intercomparison with other fluxes has been funded by the EU H2020 project SUMMER (H2020-BG-2018-2, grant agreement number 817806).

Appendix A. Supplementary data

Supplementary data to this article can be found online at https://doi.org/10.1016/j.dsr2.2023.105338.

References

Alford, M.H., Gregg, M., 2001. Near-inertial mixing: modulation of shear, strain and microstructure at low latitude. J. Geophys. Res. 106, 16 947–16 968. https://doi.org/10.1029/2000JC000370.

Arístegui, J., Duarte, C.M., Agustí, S., Doval, M., Álvarez-Salgado, X.A., Hansell, D.A., 2002. Dissolved organic carbon support of respiration in the dark ocean. Science 298 (5600). https://doi.org/10.1126/science.1076746, 1967-1967.

Baker, C.A., Henson, S.A., Cavan, E.L., Giering, S.L.C., Yool, A., Gehlen, M., Belcher, A., Riley, J.S., Smith, H.E.K., Sanders, R., 2017. Slow-sinking particulate organic carbon in the Atlantic Ocean: magnitude, flux, and potential controls. Global Biogeochem. Cycles 31, 1051–1065. https://doi.org/10.1002/2017GB005638.

Bandara, K., Varpe, Ø., Ji, R., Eiane, K., 2018. A high-resolution modeling study on diel and seasonal vertical migrations of high-latitude copepods. Ecol. Model. 368, 357–376. https://doi.org/10.1016/j.ecolmodel.2017.12.010.

Barrón, C., Duarte, C.M., 2015. Dissolved organic carbon pools and export from the coastal ocean. Global Biogeochem. Cycles 29 (10), 1725–1738. https://doi.org/10.1002/2014GB005056.

Berelson, W.M., 2001. Particle settling rates increase with depth in the ocean. Deep Sea Res. Part II Top. Stud. Oceanogr. 49 (Issues 1–3), 237–251. https://doi.org/10.1016/S0967-0645(01)00102-3. ISSN 0967-0645.

Bisson, K., Siegel, D.A., DeVries, T., 2020. Diagnosing mechanisms of ocean carbon export in a satellite-based food web model. Front. Mar. Sci. 7, 505. https://doi.org/10.3389/fmars.2020.00505.

Boyd, P.W., Claustre, H., Levy, M., et al., 2019. Multi-faceted particle pumps drive carbon sequestration in the ocean. Nature 568, 327–335. https://doi.org/10.1038/s41586-019-1098-2.

Bray, N.A., Fofonoff, N.P., 1981. Available potential energy for MODE eddies. J. Phys. Oceanogr. 11, 30–47. https://doi.org/10.1175/1520-0485(1981)011,0030:APEFME.2.0.CO;2/.

Briggs, N., Perry, Mary Jane, Cetinić, Ivona, Lee, Craig, D'Asaro, Eric, Gray, Amanda M., Rehm, Eric, 2011. High-resolution observations of aggregate flux during a sub-polar North Atlantic spring bloom. Deep Sea Res. Oceanogr. Res. Pap. 58 (Issue 10), 1031–1039. https://doi.org/10.1016/j.dsr.2011.07.007. ISSN 0967-0637.

Buesseler, K.O., Antia, A.N., Chen, M., Fowler, S.W., Gardner, W.D., Gustafsson, O., et al., 2007. An assessment of the use of sediment traps for estimating upper ocean particle fluxes. J. Mar. Res. 65 (3), 345–416. https://doi.org/10.1357/002224007781567621.

Carlson, C.A., Hansell, D.A., Nelson, N.B., Siegel, D.A., Smethie, W.M., Khatiwala, S., et al., 2010. Dissolved organic carbon export and subsequent remineralization in the mesopelagic and bathypelagic realms of the North Atlantic basin. Deep Sea Res. Part II Top. Stud. Oceanogr. 57 (16), 1433–1445. https://doi.org/10.1016/j.dsr2.2010.02.013.

CMEMS DUACS data, 2022. SEALEVEL_GLO_PHY_L4_MY_008_047. https://doi.org/10.48670/moi-00148.

CMEMS GLORYS12V1 data, 2022. GLOBAL_MULTIYEAR_PHY_001_030. https://doi.org/10.48670/moi-00021.

Cook, K.B., Belcher, A., Bondyale Juez, D., Stowasser, G., Fielding, S., Saunders, R.A., Elsafi, M.A., Wolff, G.A., Blackbird, S.J., Tarling, G.A., Mayor, D.J., 2023. Carbon budgets of Scotia Sea mesopelagic zooplankton and micronekton communities during austral spring. Deep Sea Res. Part II Top. Stud. Oceanogr. 210, 105296 https://doi.org/10.1016/j.dsr2.2023.105296. ISSN 0967-0645.

del Giorgio, P., Duarte, C., 2002. Respiration in the open ocean. Nature 420, 379–384. https://doi.org/10.1038/nature01165.

Dall'Olmo, G., Dingle, J., Polimene, L., et al., 2016. Substantial energy input to the mesopelagic ecosystem from the seasonal mixed-layer pump. Nat. Geosci. 9, 820–823. https://doi.org/10.1038/ngeo2818.

Dall'Olmo, G., Mork, K.A., 2014. Carbon export by small particles in the Norwegian Sea. Geophys. Res. Lett. 41, 2921–2927. https://doi.org/10.1002/2014GL059244.

DeVries, T., Weber, T., 2017. The export and fate of organic matter in the ocean: new constraints from combining satellite and oceanographic tracer observations. Global Biogeochem. Cycles 31 (3), 535–555. https://doi.org/10.1002/2016GB005551.

Ducklow, H.W., Steinberg, D.K., Buesseler, K.O., 2001. Upper ocean carbon export and the biological pump. Oceanography 14 (4), 50–58. https://doi.org/10.5670/oceanog.2001.06.

GEBCO Bathymetric Compilation Group, 2021. The GEBCO_2021 Grid - a Continuous Terrain Model of the Global Oceans and Land. https://doi.org/10.5285/c6612cbe-50b3-0cff-e053-6c86abc09f8f, 19 July 2021.

Giering, S.L.C., Sanders, R., Blackbird, S.J., Briggs, N., Carvalho, F., East, H., Espinola, B., Henson, S., Kiriakoulakis, K., Iversen, M.H., Klawonn, I., Lampitt, R.S., Parbotsava, K., Pebody, C., Peele, K., Preece, C., Saw, K., Stinchcombe, M., Villa, M., Wolff, G.A., 2023. Vertical imbalance in organic carbon budgets is indicative of a missing vertical transfer during a phytoplankton bloom near South Georgia (COMICS) , Deep-Sea Research II. this issue. https://doi.org/10.1016/j.dsr2.2023.105277.

Giering, S.L.C., Sanders, R., Martin, A.P., Lindemann, C., Möller, K.O., Daniels, C.J., Mayor, D.J., St John, M.A., 2016. High export via small particles before the onset of the North Atlantic spring bloom. J. Geophys. Res. Oceans 121, 6929–6945. https://doi.org/10.1002/2016JC012048.

Gregg, M.C., Sanford, T.B., Winkel, D.P., 2003. Reduced mixing from the breaking of internal waves in equatorial waters. Nature 422, 513–515. https://doi.org/10.1038/nature01507.

Hansell, D.A., 2002. Chapter 15 - DOC in the global ocean carbon cycle, 685-715. In: Hansell, Dennis A., Carlson, Craig A. (Eds.), Biogeochemistry of Marine Dissolved Organic Matter. Academic Press. https://doi.org/10.1016/B978-012323841-2/50017-8, 9780123238412.

Hansell, D.A., Carlson, C.A., 2001. Marine dissolved organic matter and the carbon cycle. Oceanography 14 (4), 41–49. https://doi.org/10.5670/oceanog.2001.05.

Hansell, D.A., Carlson, C.A., Repeta, D.J., Schlitzer, R., 2009. Dissolved organic matter in the ocean: a controversy stimulates new insights. Oceanography 22, 202–211. https://doi.org/10.5670/oceanog.2009.109.

Hansell, D.A., Carlson, C.A. (Eds.), 2014. Biogeochemistry of Marine Dissolved Organic Matter. Academic Press. https://doi.org/10.1016/C2012-0-02714-7, 978-0-12-405940-5.

Hansell, D.A., Orellana, M.V., 2021. Dissolved organic matter in the global ocean: a primer. Gels 7, 128. https://doi.org/10.3390/gels7030128.

Hansell, Dennis A., Carlson, Craig A., Amon, Rainer M.W., Álvarez-Salgado, X. Antón, Yamashita, Youhei, Romera-Castillo, Cristina, Bif, Mariana B., 2021. Compilation of Dissolved Organic Matter (DOM) Data Obtained from the Global Ocean Surveys from 1994 to 2020 (NCEI Accession 0227166). NOAA National Centers for Environmental Information. Dataset. https://doi.org/10.25921/s4f4-ye35 data download available at: https://explore.webodv.awi.de/ocean/biogeochemistry/dom/hansell-etal-2021/. (Accessed 26 July 2022).

Henson, S.A., Briggs, N., Carvalho, F., Manno, C., Mignot, A., Thomalla, S., 2023. A seasonal transition in biological carbon pump efficiency in the northern Scotia Sea, Southern Ocean. Deep Sea Res. Part II Top. Stud. Oceanogr. 208, 105274 https://doi.org/10.1016/j.dsr2.2023.105274 this issue.

Henson, S.A., Laufkötter, C., Leung, S., et al., 2022. Uncertain response of ocean biological carbon export in a changing world. Nat. Geosci. 15, 248–254. https://doi.org/10.1038/s41561-022-00927-0.

Holte, J., Talley, L.D., Gilson, J., Roemmich, D., 2017. An Argo mixed layer climatology and database. Geophys. Res. Lett. 44, 5618–5626. https://doi.org/10.1002/2017GL073426. Argo mixed layer data download: http://mixedlayer.ucsd.edu/.

Johnson, R., Strutton, P.G., Wright, S.W., McMinn, A., Meiners, K.M., 2013. Three improved satellite chlorophyll algorithms for the Southern Ocean. J. Geophys. Res.: Oceans 118 (7), 3694–3703. https://doi.org/10.1002/jgrc.20270.

Kunze, E., Firing, E., Hummon, J.M., Chereskin, T.K., Thurnherr, A.M., 2006. Global abyssal mixing inferred from lowered ADCP shear and CTD strain profiles. J. Phys. Oceanogr. 36, 1553–1576. https://doi.org/10.1175/JPO2926.1.

Kwon, E.Y., Primeau, F., Sarmiento, J.L., 2009. The impact of remineralization depth on the air–sea carbon balance. Nat. Geosci. 2 (9), 630–635. https://doi.org/10.1038/ngeo612.

Lam, P.J., Doney, S.C., Bishop, J.K., 2011. The dynamic ocean biological pump: insights from a global compilation of particulate organic carbon, CaCO3, and opal concentration profiles from the mesopelagic. Global Biogeochem. Cycles 25 (3). https://doi.org/10.1029/2010GB003868.

Ledwell, J.R., St Laurent, L.C., Girton, J.B., Toole, J.M., 2011. Diapycnal mixing in the antarctic circumpolar current. J. Phys. Oceanogr. 41 (1), 241–246. https://doi.org/10.1175/2010JPO4557.1.

Marshall, J., Speer, K., 2012. Closure of the meridional overturning circulation through Southern Ocean upwelling. Nat. Geosci. 5, 171–180. https://doi.org/10.1038/ngeo1391.

Matano, R.P., Combes, V., Young, E.F., Meredith, M.P., 2020. Modeling the impact of ocean circulation on chlorophyll blooms around South Georgia, Southern Ocean. J. Geophys. Res.: Oceans 125, e2020JC016391. https://doi.org/10.1029/2020JC016391.

Mentges, A., Feenders, C., Deutsch, C., et al., 2019. Long-term stability of marine dissolved organic carbon emerges from a neutral network of compounds and microbes. Sci. Rep. 9, 17780 https://doi.org/10.1038/s41598-019-54290-z.

Meyer, A., Sloyan, B.M., Polzin, K.L., Phillips, H.E., Bindoff, N.L., 2015. Mixing variability in the Southern Ocean. J. Phys. Oceanogr. 45 (4), 966–987. https://doi.org/10.1175/JPO-D-14-0110.1.

Munk, W., 1981. Internal waves and small-scale process. In: Evolution of Physical Oceanography: Scientific Surveys in Honor of Henry Stommel. MIT Press, 264–291.

Naveira Garabato, A.C.N., Polzin, K.L., King, B.A., Heywood, K.J., Visbeck, M., 2004. Widespread intense turbulent mixing in the Southern Ocean. Science 303 (5655), 210–213. https://doi.org/10.1126/science.1090929.

Nowicki, M., DeVries, T., Siegel, D.A., 2022. Quantifying the carbon export and sequestration pathways of the ocean's biological carbon pump. Global Biogeochem. Cycles 36, e2021GB007083. https://doi.org/10.1029/2021GB007083.

Omand, M.M., D'Asaro, E.A., Lee, C.M., Perry, M.J., Briggs, N., Cetinić, I., Mahadevan, A., 2015. Eddy-driven subduction exports particulate organic carbon from the spring bloom. Science 348 (6231), 222–225. https://doi.org/10.1126/science.1260062.

Osborn, T.R., 1980. Estimates of the local rate of vertical diffusion from dissipation estimates. J. Phys. Oceanogr. 10, 83–89. https://doi.org/10.1175/1520-0485(1980)010<0083:EOTLRO>2.0.CO;2.

Polzin, K.L., Toole, J.M., Schmitt, R.W., 1995. Finescale parameterizations of turbulent dissipation. J. Phys. Oceanogr. 25, 306–328. https://doi.org/10.1175/1520-0485(1995)025<0306:FPOTD>2.0.CO;2.

Portela, E., Kolodziejczyk, N., Vic, C., Thierry, V., 2020. Physical mechanisms driving oxygen subduction in the global ocean. Geophys. Res. Lett. 47 (17), e2020GL089040 https://doi.org/10.1029/2020GL089040.

Proteus user manual, 2023 (accessed 27/06/2023) for the Proteus Dissolved/Total Organic Carbon (DOC/TOC) sensor. https://proteus-instruments.com/parameters/dissolved-organic-carbon-doc-sensors/. (Accessed 27 June 2023).

Resplandy, L., Lévy, M., McGillicuddy Jr., D.J., 2019. Effects of eddy-driven subduction on ocean biological carbon pump. Global Biogeochem. Cycles 33, 1071–1084. https://doi.org/10.1029/2018GB006125.

Roshan, S., DeVries, T., 2017. Efficient dissolved organic carbon production and export in the oligotrophic ocean. Nat. Commun. 8, 2036. https://doi.org/10.1038/s41467-017-02227-3.

Saba, G.K., Burd, A.B., Dunne, J.P., Hernández-León, S., Martin, A.H., Rose, K.A., Salisbury, J., Steinberg, D.K., Trueman, C.N., Wilson, R.W., Wilson, S.E., 2021. Toward a better understanding of fish-based contribution to ocean carbon flux. Limnol. Oceanogr. 66, 1639–1664. https://doi.org/10.1002/lno.11709.

Sallée, J., Speer, K., Rintoul, S., Wijffels, S., 2010. Southern Ocean thermocline ventilation. J. Phys. Oceanogr. 40 (3), 509–529. https://doi.org/10.1175/2009JPO4291.1. Retrieved Jul 19, 2022.

Santana-Falcón, Y., Álvarez-Salgado, X.A., Pérez-Hernández, M.D., et al., 2017. Organic carbon budget for the eastern boundary of the North Atlantic subtropical gyre: major role of DOC in mesopelagic respiration. Sci. Rep. 7, 10129 https://doi.org/10.1038/s41598-017-10974-y.

Sarmiento, J.L., Gruber, N.P., 2006. Ocean biogeochemical dynamics. In: Ocean Biogeochemical Dynamics. Princeton University Press, 9780691017075.

Sheen, K.L., Brearley, J.A., Naveira Garabato, A.C., Smeed, D.A., Waterman, S., Ledwell, J.R., et al., 2013. Rates and mechanisms of turbulent dissipation and mixing in the Southern Ocean: results from the diapycnal and isopycnal mixing experiment in the Southern Ocean (DIMES). J. Geophys. Res.: Oceans 118 (6), 2774–2792. https://doi.org/10.1002/jgrc.20217.

Siegel, D.A., Buesseler, K.O., Behrenfeld, M.J., Benitez-Nelson, C.R., Boss, E., Brzezinski, M.A., Burd, A., Carlson, C.A., D'Asaro, E.A., Doney, S.C., Perry, M.J., Stanley, R.H.R., Steinberg, D.K., 2016. "Prediction of the export and fate of global ocean net primary production: the EXPORTS science plan". Front. Mar. Sci. https://doi.org/10.3389/fmars.2016.00022.

Siegel, D.A., DeVries, T., Doney, S.C., Bell, T., 2021. Assessing the sequestration time scales of some ocean-based carbon dioxide reduction strategies. Environ. Res. Lett. 16 (10), 104003 https://doi.org/10.1088/1748-9326/ac0be0.

Steinberg, D.K., Landry, M.R., 2017. Zooplankton and the ocean carbon cycle. Ann. Rev. Mar. Sci 9 (1), 413–444. https://doi.org/10.1146/annurev-marine-010814-015924.

Stukel, M.R., Ducklow, H.W., 2017. Stirring up the biological pump: vertical mixing and carbon export in the Southern Ocean. Global Biogeochem. Cycles 31 (9), 1420–1434. https://doi.org/10.1002/2017GB005652.

Stukel, M.R., Décima, M., Landry, M.R., 2022. Quantifying biological carbon pump pathways with a data-constrained mechanistic model ensemble approach. Biogeosciences 19, 3595–3624. https://doi.org/10.5194/bg-19-3595-2022.

Suess, E., 1980. Particulate organic carbon flux in the oceans—surface productivity and oxygen utilization. Nature 288 (5788), 260–263. https://doi.org/10.1038/288260a0.

Thompson, A.F., Gille, S.T., MacKinnon, J.A., Sprintall, J., 2007. Spatial and temporal patterns of small-scale mixing in Drake Passage. J. Phys. Oceanogr. 37 (3), 572–592. https://doi.org/10.1175/JPO3021.1.

Thurnherr, A.M., 2021. How to Process LADCP Data with the LDEO Software, Version IX.14. Lamont Doherty Earth Observatory.

Turner, Jefferson T., 2015. Zooplankton fecal pellets, marine snow, phytodetritus and the ocean's biological pump. Prog. Oceanogr. 130, 205–248. https://doi.org/10.1016/j.pocean.2014.08.005. ISSN 0079-6611.

Visbeck, M., 2002. Deep velocity profiling using lowered acoustic Doppler current profilers: bottom track and inverse solutions. J. Atmos. Ocean. Technol. 19, 794–807. https://doi.org/10.1175/1520-0426(2002)019<0794:DVPULA>2.0.CO;2[.

Wagner, S., Schubotz, F., Kaiser, K., Hallmann, C., Waska, H., Rossel, P.E., et al., 2020. Soothsaying DOM: a current perspective on the future of oceanic dissolved organic carbon. Front. Mar. Sci. 7, 341. https://doi.org/10.3389/fmars.2020.00341.

Waterhouse, A.F., Coauthors, 2014. Global patterns of dia- pycnal mixing from measurements of the turbulent dissipation rate. J. Phys. Oceanogr. 44, 1854–1872. https://doi.org/10.1175/JPO-D-13-0104.1.

Wu, L., Jing, Z., Riser, S., et al., 2011. Seasonal and spatial variations of Southern Ocean diapycnal mixing from Argo profiling floats. Nat. Geosci. 4, 363–366. https://doi.org/10.1038/ngeo1156.